Blocking toxin function and modulating the gut microbiota: caffeic acid phenethyl ester as a potential treatment for *Clostridioides difficile* infection

Yan Guo[1#], Yong Zhang[2#], Guizhen Wang[3], Hongtao Liu[1], Jianfeng Wang[1], Xuming Deng[1], Liuqing He[4*], Jiazhang Qiu[1*]

[1] State Key Laboratory for Diagnosis and Treatment of Severe Zoonotic Infectious Diseases, Key Laboratory for Zoonosis Research of the Ministry of Education, College of Veterinary Medicine, Jilin University, Center for Pathogen Biology and Infectious Diseases, The First Hospital of Jilin University, Changchun, China.

[2] Center for Pathogen Biology and Infectious Diseases, State Key Laboratory for Zoonotic Diseases, The First Hospital of Jilin University, Changchun 130021, China.

[3] Measurement Biotechnique Research Center, College of Biological and Food Engineering, Jilin Engineering Normal University, Changchun 130052, China.

[4] Hunan Provincial Key Laboratory of Animal Intestinal Function and Regulation, Hunan International Joint Laboratory of Animal Intestinal Ecology and Health, Laboratory of Animal Nutrition and Human Health, College of Life Sciences, Hunan Normal University, Changsha, China.

#YG and YZ contributed equally to this work.

*Correspondence: Jiazhang Qiu (qiujz@jlu.edu.cn); Liuqin He (heliuqin@hunnu.edu.cn)

Abstract

Clostridioides difficile infection (CDI) is the leading cause of hospital-acquired diarrhea that seriously threatens public health. The disruption of normal gut microbiota by the use of broad-spectrum antimicrobial agents enables *C. difficile* to proliferate in the colon. The emergence and prevalence of hypervirulent *C. difficile* strains result in increased morbidity, mortality, and high recurrence rates of CDI, thus creating a pressing need for novel therapeutics. The multi-domain toxins TcdA and TcdB are the primary determinants of CDI pathogenesis, rendering them ideal drug targets in the anti-virulence paradigm. In this study, we identified caffeic acid and its derivatives from natural compounds library as active inhibitors of TcdB via a cell-based high-throughput phenotypic screening. Further mechanistic investigations revealed that caffeic acid phenethyl ester (CAPE) could directly bind to TcdB, thus suppressing $InsP_6$-induced autoproteolysis and inhibiting glucosyltransferase activity. CAPE treatment remarkably reduces the pathology of CDI in a murine infection model in terms of alleviated diarrhea symptoms, decreased bacterial colonization, and relieved histopathological lesions. Moreover, CAPE treatment of *C. difficile*-challenged mice induces a remarkable increase in the diversity and composition of the gut microbiota and alterations of gut metabolites (e.g., adenosine, D-proline, and melatonin), which might partially contribute to the therapeutic outcomes of CAPE against CDI. Our results reveal the potential of CAPE as a therapeutic for the

management of CDI, or CAPE might serve as a lead compound for the development of antivirulence drugs targeting TcdB.

Keywords: *Clostridioides difficile*; toxin B; caffeic acid phenethyl ester; gut microbiota; gut metabolites

Introduction

Clostridioides difficile (*C. difficile*) is an obligate anaerobic, spore-forming, gram-positive bacterial pathogen that is the most common cause of hospital-acquired and antibiotic-associated gastrointestinal diseases, including mild diarrhea and life-threatening pseudomembranous colitis [1, 2, 3]. In the United States, *C. difficile* is responsible for almost half a million infections and approximately 29,000 deaths per year, resulting in an estimated annual healthcare-associated cost of up to $4.8 billion [4, 5]. Importantly, the incidence, severity, mortality and healthcare costs of *C. difficile* infection (CDI) have dramatically increased in the 21st century, at least partially owing to the frequent use of antimicrobial agents and the emergence of hypervirulent strains (e.g., PCR ribotypes 027 and 078) [6, 7, 8]. Limited options are available for the treatment of CDI, while antibiotics including metronidazole, fidaxomicin and vancomycin, are the mainstays of clinical practice [9, 10]. However, antibiotic treatment is ineffective in more than 35% of CDI patients and can lead infection recurrence [11, 12]. Moreover, the rapid evolution of antibiotic resistance in *C. difficile* has further compromised the therapeutic efficacy of current treatment options [13]. Therefore, the high morbidity and mortality, high recurrence rates, and emergence of multiple antibiotic-resistant isolates have made this pathogen a major threat to public health; these factors highlight the urgent need for novel therapies.

C. difficile widely exists in the environment and in the intestinal tract of

humans and animals and is mainly transmitted via the fecal-oral route [14]. The pathogenesis of CDI is correlated with the use of antibiotics, which impair the structure and composition of the normal gut microbiota, thus allowing *C. difficile* to proliferate in the colon [14]. Therefore, previous antibiotic therapy is the major risk factor for the development of CDI. In the colon, the dormant spores of *C. difficile* germinate into oxygen-sensitive vegetative cells that produce toxins and cause symptoms of disease [15]. *C. difficile* secretes two large clostridial exotoxins (TcdA and TcdB), which are directly responsible for the clinical pathology of CDI [16, 17]. Epidemiological studies suggest that most disease-causing *C. difficile* strains have genes that encode TcdB [18, 19]. TcdA and TcdB have identical functional domains: a N-terminal glucosyltransferase catalytic domain (GTD), a cysteine protease active domain (CPD), a transmembrane domain (DRBD), and a C-terminal receptor binding domain (CROPs) [20]. When secreted into the colon, both toxins are internalized by host cells through receptor-mediated, clathrin-dependent endocytosis. Following a decrease in endosomal pH, the toxins undergo conformational changes in the DRBD, resulting in insertion of the toxin into the endosome membrane, pore formation, and the release of the GTD and CPD domains into the cytosol. Then, CPD binding with cytosolic inositol hexakisphosphate ($InsP_6$) activates its protease activity, leading to the cleavage and release of the GTD. Eventually, the GTD utilizes UDP-glucose to glucosylate Rho and/or Ras family GTPases, thus disrupting GTPase signaling and resulting in deleterious effects, including

cytopathic “rounding”, dysregulation of the actin cytoskeleton, apoptosis, and pyroptosis [1]. Although both toxins are cytotoxic to host cells, TcdB shows greater toxicity than TcdA [21].

Disruption of the gut microbiota by antimicrobial agents results in high recurrence rates, which limits the application of antimicrobial therapy for CDI [14]. Consequently, there is a critical need to develop nonantibiotic treatments for CDI, either as standalone or augmented therapies. Importantly, strategies targeting bacterial virulence factors, including toxins, are termed anti-virulence strategies and have attracted interest in the 21st century [22]. Owing to its essential role in *C. difficile* pathogenesis, TcdB has become an ideal target for the development of anti-virulence drugs [23]. In this study, caffeic acid and a series of its derivatives were found to inhibit TcdB-mediated cell rounding via cell-based screening. Among these potential inhibitors, caffeic acid phenethyl ester (CAPE) had the greatest inhibitory effect. Mechanistically, CAPE bound to both full-length TcdB and the GTD fragment, leading to alterations in the secondary structure. This interaction suppressed the $InsP_6$-mediated self-cleavage of TcdB, as well as the enzymatic activity of GTD, thereby decreasing the level of glucosylated Rac1 in TcdB-treated host cells and further inhibiting the cytopathology and cytotoxicity of TcdB. Oral administration of CAPE significantly protected against CDI in models of animal infection. In addition to direct toxin inhibition, the therapeutic effect may also be attributed to CAPE-induced alteration of the gut microbiota (e.g., *Bacteroides*

spp.) as well as gut metabolites (e.g., adenosine, D-proline, and melatonin). Overall, our study revealed that caffeic acid and its derivatives, particularly CAPE, may serve as promising lead compounds for the development of anti-virulence drugs to treat CDI.

Results

CAPE inhibits cell rounding induced by TcdB

TcdB can inactivate Rho GTPases via glucosylation, leading to the loss of cytoskeletal structure and cell-rounding. Consequently, we utilized this phenotype to identify potential TcdB inhibitors from 2076 chemicals, including 1515 FDA-approved drugs and 561 natural compounds. The minimal concentration of recombinant His_6-TcdB (0.2 ng/mL) that induced 100% cell rounding within 1 h was used for drug screening. This concentration of TcdB was preincubated with 8 μg/mL of the individual compounds for 1 h, the compounds that were not bound to TcdB were removed by ultrafiltration centrifugal partition and then added to Vero cell cultures. Residual compounds that have not bound to TcdB may lead to an exaggerated assessment of their efficacy and could also result in misleading positive outcomes. As the effective concentration for cellular interactions may inadvertently be increased, such carryover could distort the determination of the compound's minimum effective concentration. At 1 h post-TcdB treatment, cell morphology was visualized under a light microscope (**Figure 1A**). These analyses allowed us to identify

22 candidate compounds with potent inhibitory effects (**Figure 1B**). Interestingly, six out of the 22 compounds were caffeic acid derivatives. The natural compound library contained eight caffeic acid derivatives, of which methyl caffeic acid and ferulic acid displayed no efficacy. Caffeic acid itself only slightly inhibited TcdB-induced cell rounding, with a 50% inhibitory concentration (IC_{50}) of 527.5 μg/mL (1.86 mM) (**Table S1**). Notably, except for rosmarinic acid, the IC_{50} values for the other screened caffeic acid derivatives were less than 6 μg/mL, suggesting that these compounds potently inhibited TcdB-mediated toxicity (**Table S1**). CAPE is the phenethyl alcohol ester of caffeic acid and a main active component of propolis with broad pharmacological properties, such as anticancer, anti-inflammatory, antiviral, antibacterial, antifungal, antioxidant, and immunomodulatory activities [24]. As CAPE has the lowest IC_{50} (3.0 μg/mL) among the active caffeic acid derivatives, it was selected as the representative compound for subsequent investigations (**Table S1**). After preincubation with increasing concentrations of CAPE, dose-dependent inhibition of cell rounding was observed in both Vero and HeLa cells (**Figure 1C**). The protective influence of CAPE against TcdB-induced Vero cell death remained evident even when the treatment duration was prolonged to 12 h (**Figure S1A-B**).

In addition, we also determined whether inhibition of TcdB by CAPE could lead to loss of toxin function *in vivo* using a murine systemic intoxication model. A lethal dose of recombinant His_6-TcdB (30 ng) was preincubated with either

DMSO or CAPE (2 or 4 μg/mL) for 1 h at 37 ^{o}C, followed by intraperitoneal injection into mice. Notably, all mice in the DMSO group (n=10) died within 36 h after toxin injection. However, 100% of mice pretreated with CAPE 4 (μg/mL) toxin survived at the monitoring endpoint (72 h) (n=10) (**Figure 1D**). Furthermore, we evaluated the efficacy of CAPE following an intraperitoneal injection by administering it 2 h prior to the injection of TcdB, in order to gauge the survival rate of the mice. The outcomes revealed that a 2 h pretreatment with CAPE at doses of 30 and 50 mg/kg significantly enhanced the mice's protection rate by 57.1% (**Figure S2)**. Simultaneously, we assessed the impact of CAPE on *C.difficile* itself. CAPE markedly repressed *tcdB* gene expression at a concentration of 16 μg/mL (**Figure S3A**) and inhibited the growth and spore formation of *C. difficile* BAA-1870 at a concentration of 32 μg/mL (**Figure S3B-C**). Taken together, these data indicate that CAPE is a potent toxin inhibitor of TcdB and may serve as a promising antimicrobial agent.

CAPE decreases $InsP_6$-induced autoproteolysis of TcdB and inhibits the enzymatic activity of GTD

TcdB is a multi-domain containing toxin that induces toxicity in host cells via an intricate and multistep mechanism. This mechanism involves (i) receptor-mediated endocytosis, (ii) pore formation and subsequent membrane translocation, (iii) autoproteolysis and release of GTD, and (iv) the glucosylation of small GTPases (**Figure 2A**). To determine the mechanism by

186 which CAPE suppresses the cytotoxicity of TcdB, we first labeled full-length
187 TcdB with Alexa Fluor 488; then, the concentration of the endocytosed toxin
188 was determined via flow cytometry. Apparently, incubation of CAPE with TcdB
189 did not significantly affect its entry into host cells (**Figure 2B**). Next, we stained
190 CAPE-treated cells with LysoTracker, a fluorescent dye that accumulates in
191 the acidic organelles of live cells. In contrast to the vacuolar-type H+-ATPase
192 (V-ATPase) inhibitor bafilomycin A1 (Baf-A1), CAPE treatment did not alter the
193 intensity of LysoTracker fluorescence staining in either THP-1 or Caco-2 cells,
194 suggesting that inactivation of TcdB by CAPE is not due to changes in the pH
195 of endosomal compartments (**Figure 2C-D** and **Figure S4A-B**).

196 These observations indicate that CAPE might exert its effects after
197 membrane translocation. Indeed, preincubation of full-length TcdB with CAPE
198 blocked the $InsP_6$-induced autoproteolysis of TcdB, as revealed by the gradual
199 decrease in the production of released GTP, followed by the addition of
200 increasing amounts of CAPE *in vitro* (**Figure 2E-F**). Furthermore, we
201 determined the glucosyltransferase activity using recombinant GTD in the
202 absence or presence of different doses of CAPE. Strikingly, incubation with 2
203 μg/mL CAPE resulted in a significant reduction in GTD activity, whereas 32
204 μg/mL CAPE compromised 87.5% of the enzymatic activity (**Figure 2G**).
205 Importantly, in response to suppression of $InsP_6$-induced autoproteolysis and
206 GTD function, treatment of TcdB-challenged cells with CAPE markedly
207 decreased the level of glucosylated Rac1 in a dose-dependent manner

(**Figure 2H-I**). Taken together, these results suggest that CAPE disrupts $InsP_6$-induced autoproteolysis of TcdB and inhibits the enzymatic activity of GTD, thereby decreasing the glucosylation of Rac1 and alleviating cell rounding.

CAPE alters the secondary structure of full-length TcdB and GTD

To further clarify the mechanisms used by CAPE to inactivate TcdB, we determined the secondary structures of full-length TcdB and GTD in the absence or presence of CAPE by circular dichroism spectroscopy. Apparently, incubation of CAPE with full-length TcdB resulted in a significant increase in the α-helix content (15.4% to 21.0%) and a concomitant decrease in the β-pleated sheet content (34.5% to 20.9%) (**Figure 3A-B**). Similarly, the secondary structure of GTD was markedly altered upon incubation with CAPE, with the proportion of α-helices decreasing from 37.9% to 0.0% and the proportion of β-pleated sheets decreasing from 37.2% to 10.9% (**Figure 3C-D**). Taken together, these data suggest that CAPE may interact with full-length TcdB and GTD to induce conformational changes, thus impairing their functions.

CAPE directly interacts with full-length TcdB and GTD

To investigate the potential interaction between CAPE and TcdB or GTD, the binding constants were determined by surface plasmon resonance (SPR) analysis. The results showed that CAPE has strong binding affinity with full-length TcdB and GTD, and the KD values were 1.269×10^{-5} M and

230 1.007×10^{-3} M, respectively (**Figure 4A-B**). The interaction between CAPE and
231 TcdB exhibits a slow approach to equilibrium, which may primarily be attributed
232 to the rapid occupation of the protein's primary binding sites by the small
233 molecule during the initial phase. Following this, CAPE proceeds to bind to
234 sites with secondary or reduced affinity, a process that prolongs the time
235 required to achieve equilibrium. Furthermore, the possibility that CAPE binds
236 to multiple sites on TcdB necessitates a duration for the exploration and
237 occupation of these various sites before equilibrium is established. These data
238 demonstrate the direct interaction between CAPE and full-length TcdB/GTD.

239 Next, we performed molecular docking and molecular simulation
240 dynamics analyses to investigate the interaction between CAPE and GTD
241 (**Figure 5A**). The results revealed that Leu265, Asp286, Thr465, Ile466,
242 Leu519, and Trp520 in GTD were potential binding sites for CAPE (**Figure 5A**).
243 The root mean square deviation (RMSD) of the GTD/CAPE complex was
244 stable over a 100 ns period of simulation (**Figure 5B**). Further energy
245 decomposition analysis showed that the side chains of Leu265, Thr465,
246 Leu519, and Trp520 of GTD contributed to binding with CAPE via van der
247 Waals interactions, among which Trp520 had the highest binding energy
248 (**Figure 5C**). Moreover, we mutated each of the residues that were involved in
249 binding and subsequently determined their glucosyltransferase activities in the
250 presence or absence of CAPE. The enzymatic activities of these mutants were
251 similar to that of wild-type GTD (**Figure 5D**). Mutations in GTD_{L265A}, GTD_{T465A},

252 GTD_{I466A}, and GTD_{L519A} did not affect the inhibitory effect of CAPE (**Figure**
253 **5E-I**). However, the inhibition of GTD_{W520A} and GTD_{D286A} by CAPE was notably
254 compromised (**Figure 5J-K**).

255 **CAPE treatment reduces the pathology of CDI in a murine model**

256 The abovementioned observation that CAPE suppresses the function of
257 TcdB prompted us to further evaluate the potential therapeutic effects of this
258 compound in CDI. To this end, we employed a well-established murine model
259 in which infected mice can develop symptoms resembling those observed in
260 human CDIs (25). First, cytotoxicity measurements revealed that the viability of
261 both THP-1 and Vero cells was not affected by CAPE treatment (**Figure**
262 **S5A-B**), thus indicating low toxicity. Mice were preconditioned with drinking
263 water containing 0.5 g/L cefoperazone for 5 days, followed by normal drinking
264 water for 2 days. After challenge with *C. difficile* BAA-1870 via gavage, mice
265 were then treated daily with either vehicle or 30 mg/kg CAPE by gavage
266 throughout the disease course (day 0 to day 5) (**Figure 6A**). Severe weight
267 loss in *C. difficile*-infected mice was observed on days 2 and 3 post infection
268 and was accompanied by diarrhea (**Figure 6B**). Notably, compared to the
269 infection control group, CAPE treatment significantly increased the dry/wet
270 weight ratio of the mouse feces, suggesting the alleviation of diarrhea
271 symptoms (**Figure 6C**). Correspondingly, the weight loss of mice was relieved
272 upon receiving CAPE (**Figure 6B**). Moreover, fecal pellets collected on day 3
273 were used to determine the bacterial burden. The results revealed that CAPE

treatment significantly decreased the number of *C. difficile* CFUs (**Figure 6D**). On day 3 post-*C. difficile* infection, the colon was collected for histopathological analysis. Remarkably, *C. difficile*-infected mice exhibited conspicuous colon edema, epithelial cell injury and inflammatory factor infiltration (**Figure 6E**). In contrast, these histopathological lesions were significantly reduced in mice given CAPE, but pathological changes were still present (**Figure 6F**). This indicates that CAPE may have a limited capacity to reverse the histological damage induced by *C. difficile*. The residual pathology could be attributed to the complex interplay between the pathogen, the host immune response, and the tissue repair process, which may not be fully mitigated by the inhibitory effects of CAPE on TcdB.

CAPE induces distinct microbiota changes in CAPE-treated mice when compared with control mice

Antibiotic-induced dysbiosis of the gut microbiota promotes the development of CDI [25]. Therefore, we next determined whether CAPE has any impact on gut microbial communities that may contribute to its therapeutic efficacy. To this end, on the 3rd day after *C. difficile* challenge, fecal samples from the control group and CAPE treatment group were collected and subjected to microbiota analysis via 16S rRNA gene sequencing. Remarkably, as reflected by the Venn diagram, CAPE treatment resulted in significant changes in the microbial composition compared to those in the control group, and only 16.42% of the operational taxonomic units (OTUs) were shared

(**Figure 7A**). In addition, both the α- and β-diversity of the gut microbiota in CAPE-treated mice were significantly greater than those in control mice. Specifically, the increase in the Chao1 richness estimator of mice in the CAPE treatment group suggested a greater number of microbial species and increased evenness in the fecal samples (**Figure 7B-C**); the increase in the Shannon□Wiener diversity index and the Simpson diversity index reflected a significant increase in microbiota diversity (**Figure 7D-E**). Principal coordinate analysis (PCoA) revealed distinct confidence ellipses between the bacterial communities of the CAPE-treated group and the control group, thereby revealing substantial differences in their microbiota profiles (**Figure 7F**).

A comparative analysis was performed to examine changes at the phylum level following CAPE treatment. *Bacteroidota*, *Firmicutes,* and *Proteobacteria* were the major constituents in both the CAPE treatment and control groups, suggesting that the administration of CAPE did not significantly alter the mouse microbiota at the phylum level (**Figure 7G**). Next, we compared the 10 most abundant taxa at the genus level. Notably, CAPE treatment markedly elevated the abundance of *Bacteroides* and decreased the abundance of *Muribaculaceae* and *Parabacteroides* (**Figure 7H**). Leveraging linear discriminant analysis of effect sizes (LEfSe), the microbiota was examined at the genus level to identify bacteria exhibiting substantial differences in abundance between the two cohorts (LDA score > 3.5, $p < 0.05$). After CAPE treatment, the relative abundance of *Bacteroides*,

Ruminococcus_gnavus_group, *Muribaculum* and *Faecalibaculum* OTUs notably increased, while that of *Hungatella*, *Parasutterella* and *Muribaculaceae* OTUs significantly decreased (**Figure 7I**). *Bacteroides*, *Muribaculum* and *Faecalibaculum* improve colonization resistance to *C. difficile* [26, 27, 28]. Importantly, the abundance of these bacterial species increased following CAPE treatment (**Figure 7J-L**). In contrast, the abundance of *Parasutterella*, a bacterium that facilitates *C. difficile* colonization [29], was reduced in mice receiving CAPE (**Figure 7M**). Taken together, these findings suggest that the gut microbiota alteration might contribute modestly to the observed effects.

CAPE alters the levels of gut metabolites in *C. difficile*-infected mice

In addition to the crucial role of the gut microbiota in conferring colonization resistance against *C. difficile*, gut microbiota-derived metabolites significantly contribute to the disease process [30]. Metabolomic analysis was performed to evaluate the effects of CAPE treatment on gut metabolites in mice. On the 3rd day after infection, the feces of mice in each group were frozen by liquid nitrogen for metabolomics analysis. Specifically, utilizing mass spectrometry-based metabolomics, a simple screening of each metabolite is conducted for parameters such as retention time and mass-to-charge ratio. Subsequently, peak area calibration is performed using the first quality control (QC) sample to enhance the accuracy of identification. The peak extraction is then conducted with settings for mass deviation at 5 ppm, signal intensity deviation at 30%, minimum signal intensity, and adduct ions. Simultaneously,

quantification of peak areas is carried out, and target ions are integrated. Molecular formulas are predicted using molecular ion peaks and fragment ions, and these are compared with databases such as mzCloud, mzVault, and Masslist. Background ions are removed using blank samples. The raw quantification results are standardized using the formula: original quantification value of the sample / (total metabolite quantification value of the sample / total metabolite quantification value of QC1 sample), to obtain relative peak areas. Compounds with a coefficient of variation (CV) greater than 30% in the relative peak areas of QC samples are excluded. Finally, the identification and relative quantification results of the metabolites are obtained. The PLS-DA model exhibited significant separation of clusters between the model and CAPE treatment groups (**Figure 8A**). Among the 1599 metabolites, 109 showed substantial differences in levels between the two groups. Specifically, CAPE-treated mice exhibited 19 metabolites with upregulated expression and 50 metabolites with downregulated expression compared to those in the control group (fold change > 1.5, $p < 0.05$) (**Figure 8B**). Furthermore, KEGG enrichment analysis revealed that the differentially abundant metabolites were significantly enriched in the purine metabolism and bile secretion pathways (**Figure 8C**). Adenosine is an endogenous purine nucleoside that binds to specific cell surface receptors to exert anti-inflammatory effects at high concentrations [31]. Importantly, CAPE treatment of *C. difficile*-infected mice can increase the adenosine concentration in the gut (**Figure 8D**), which might be

362 attributed to its inhibition of xanthine oxidase [32]. Similarly, the levels of uric acid,
363 the final product of purine degradation, were markedly decreased in mice after
364 receiving CAPE (**Figure 8D**). An earlier study reported that increasing the gut
365 adenosine concentration with an adenosine deaminase inhibitor prevents *C.*
366 *difficile* toxin A-induced enteritis in mice [33]. Therefore, the increase in gut
367 adenosine induced by CAPE might play an important role in its therapeutic
368 efficacy in CDI.

369 *C. difficile* predominantly utilizes sugars and amino acids for energy
370 production through various metabolic pathways, such as fermentation [34].
371 Notably, Stickland fermentation, a Clostridia-specific type of amino acid
372 fermentation, is associated with *C. difficile* pathogenesis [34]. D-proline is one of
373 the preferred nutrients used by *C. difficile* in the Stickland reaction and is
374 critical for its growth [35, 36]. Interestingly, treatment of *C. difficile*-infected mice
375 with CAPE significantly reduced gut D-proline levels (**Figure 8D**). In addition,
376 the metabolomics data also revealed a dramatic increase in the level of
377 melatonin (**Figure 8D**), which is a ubiquitous indolamine that was previously
378 shown to decrease the rate of recurrent CDI [37]. Consistently, quantification of
379 the melatonin content in mouse fecal supernatants using a melatonin detection
380 kit revealed elevated levels of melatonin in CAPE-treated mice (**Figure S6**).
381 Moreover, correlation analysis revealed a positive association between
382 *Faecalibaculum* abundance and melatonin levels (**Figure S7**). Taken together,
383 these results indicate that alterations in gut metabolites caused by CAPE

treatment might contribute to its therapeutic efficacy in CDI. We found that the metabolites of the gut microbiota changed after CAPE treatment. While detectable, the impact of gut microbiota modifications seems to be of secondary importance.

Oral administration of melatonin alleviates the symptoms of CDI

Next, we investigated whether any of the upregulated metabolites had a direct influence on TcdB. To this end, we preincubated recombinant TcdB with each of the selected metabolites prior to addition to the cell cultures. Interestingly, treatment with TcdB and 100 μg/mL melatonin significantly alleviated the cell death induced by this toxin (**Figure 9A**). This observation prompted us to investigate the direct therapeutic potential of melatonin in CDI. Therefore, *C. difficile*-infected mice were orally administered 200 mg/kg melatonin at 24 h intervals. The weight changes and the dry/wet ratio of the stool samples were monitored daily for three days. The results showed that melatonin-treated mice displayed remarkable alleviation of diarrhea, as manifested by notable improvements in weight recovery and a significant increase in the dry/wet weight ratio on the 2nd and 3rd days after *C. difficile* challenge (**Figure 9B-C**). Consistent with these observations, histopathological assessment of colonic tissue sections also revealed attenuated colon damage upon melatonin treatment (**Figure 9D-E**). Taken together, these data indicate that a high dose of exogenous melatonin could protect mice from CDI, However, the CAPE treatment group induced only

minor alterations in gut microbiota-derived melatonin levels, which may not reach therapeutic relevance. While existing studies suggest that melatonin exhibits beneficial effects against CDI, the primary antimicrobial activity appears to be mediated directly by CAPE rather than through melatonin-associated mechanisms.

Discussion

C. difficile has become the prevalent agent of nosocomial diarrhea and substantially threatens public health. In particular, the increase in morbidity and mortality caused by the prevalence of hypervirulent and drug-resistant strains has become a global concern [7]. In 2019, *C. difficile* was listed by the US Centers for Disease Control and Prevention as an “urgent threat” that surpassed methicillin-resistant *Staphylococcus aureus* (MRSA) and ESBL-producing *Enterobacterales* [38]. *C. difficile* is a commensal bacterium that colonizes the lower gastrointestinal tract [39]. CDI typically occurs in susceptible individuals whose normal gut microbiota is disrupted by the administration of broad-spectrum antibiotics [39]. Although CDI is considered an antibiotic-associated disease, the current treatment for CDI still relies on antimicrobial drugs, including metronidazole, fidaxomicin and vancomycin [9, 10]. Despite antibiotic therapy, more than 35% of CDI patients are susceptible to recurrent infection, which is primarily attributable to the intrinsic effects of antimicrobial agents, which disrupt the microbiota [12]. In addition, long-term

428 administration of antibiotics promotes the selection of antibiotic-resistant
429 subpopulations in the gut, thus increasing the risk of infections caused by
430 antibiotic-resistant and opportunistic bacteria [40]. As a result, the development
431 of nonantibiotic therapeutics is needed for the treatment of CDI.

432 Indeed, numerous novel treatments for CDI are being investigated, among
433 which the anti-virulence strategy represents one of the most promising and
434 successful therapeutic approaches [22, 41]. Unlike antibiotics, which target
435 bacterial components that are critical for bacterial growth, anti-virulence drugs
436 aim to disarm pathogenic bacteria by neutralizing their virulence factors [42, 43].
437 Therefore, this strategy imposes less selective pressure that directs bacterial
438 evolution of antimicrobial resistance [43]. The disease progression of CDI is
439 strictly dependent on large clostridial toxins (TcdA and TcdB), as strains lacking
440 both toxins (i.e., A^-B^-) were completely avirulent and failed to induce any
441 discernable disease symptoms in a hamster model of infection [44]. Importantly,
442 epidemic *C. difficile* strains with increased morbidity and mortality rates
443 produce greater amounts of toxins [45]. Based on these premises, TcdA and
444 TcdB are considered ideal drug targets for CDI in the anti-virulence paradigm
445 [46]. Indeed, bezlotoxumab, a fully humanized monoclonal antibody that
446 neutralizes TcdB, was approved by the FDA and used in CDI patients to
447 reduce the rate of recurrence [47]. This achievement has encouraged
448 researchers to develop next-generation anti-virulence treatments. In particular,
449 small molecule inhibitors of toxin production and/or activity have attracted

increasing interest owing to their advantages in cost and the convenience of oral administration [41]. The multidomain architecture and mechanisms of action of clostridial toxins have provided distinct options for blocking their toxicity. Indeed, previous efforts have identified diverse inhibitors that act on distinct steps of intoxication, such as the inhibition of toxin binding to cell receptors, the suppression of endosomal maturation, and the inactivation of GTD or CPD activities [23, 48, 49, 50, 51]. Although which approach is the best remains unknown, we believe that an inhibitor that targets multiple steps of intoxication would be superior to those that act on a single step. In this study, we identified a series of caffeic acid derivatives that were potent inhibitors of TcdB via a phenotypic screen. Further mechanistic study revealed that CAPE, the phenethyl alcohol ester of caffeic acid, could block $InsP_6$-induced autoproteolysis of TcdB and inactivate its GTD function (**Figure 10**). CAPE can also inhibit the growth of *C. difficile* and the production of spores. Moreover, CAPE treatment significantly protected against CDI in a mouse model of infection. Our results suggested that caffeic acid derivatives, particularly CAPE, are promising lead compounds for the development of targeted therapies against CDI. CAPE is a major component of propolis, a natural bee-produced substance that has been used as a remedy for thousands of years in Europe and Asia [52]. As a result, further investigations on the therapeutic potential of propolis against CDI, either in combination with standard therapy or as a single therapy, would be of great interest.

Antibiotic-induced gut microbiota dysbiosis is a major risk factor for CDI [53]. Thus, reconstituting the gut microbiota is a promising strategy for CDI therapy. Fecal microbiota transplantation (FMT) is considered an effective CDI therapeutic strategy and is widely used in clinical practice [54]. Despite the high cure rate and increasing popularity of FMT, patients remains limited acceptance. Another prominent advantage of anti-virulence drugs is that they allow maintenance of the normal microbiota, which is of critical importance for the treatment of CDI. Importantly, CAPE treatment of *C. difficile*-infected mice restored the structure and composition of the microbiota (**Figure 10**). In particular, the abundance of *Bacteroides*, a critical gut microbiota component that is required for resistance to *C. difficile* colonization [26, 55, 56, 57], was significantly elevated upon CAPE treatment. Interestingly, *Bacteroides* were also predominant in CDI patients administered RBX2660 (Rebyota), an FDA-approved fecal microbiota product [58, 59]. The increased diversity of the gut microbiota might contribute to the therapeutic effects of CAPE in CDI.

In addition to the microbiota, gut metabolites also play crucial roles in the pathogenesis of CDI, either by promoting or suppressing disease progression [30]. For example, bile acids and amino acids promote spore germination and pathogenesis, while secondary bile acid and short-chain fatty acids aid in colonization resistance and suppress spore germination [30]. In addition to restoration of the gut microbiota, metabolomics analysis of mouse fecal samples revealed dramatic alterations in gut metabolites upon CAPE

treatment (**Figure 10**). The differentially abundant metabolites were significantly enriched in the purine metabolism and bile metabolism pathways. Remarkably, the level of adenosine, an endogenous purine nucleoside that can regulate immune responses and inflammatory processes by binding to its receptors, such as its ability to inhibit the release of certain inflammatory mediators, was dramatically increased in CAPE-treated mice [60, 61]. In contrast, the amount of uric acid, the final product of purine metabolism, was reduced. Previous studies showed that the increase in adenosine concentrations caused by the inhibition of adenosine deaminase via EHNA prevents *C. difficile* TcdA-mediated damage and inflammation [33]. This protection might be a result of the anti-inflammatory effects of adenosine, which rely on the activation of its receptors [62]. In addition, we observed a reduction in the amount of D-proline, which is one of the preferred amino acids utilized by *C. difficile* to generate energy through Stickland reactions [35]. Melatonin is a ubiquitous indolamine that has broad biological activities [63]. Notably, we detected a significantly increase in the amount of melatonin in the feces of mice that were administered CAPE. Importantly, an earlier study demonstrated a decreased risk of recurrent CDI in patients exposed to melatonin, possibly owing to its antibacterial and anti-inflammatory activities [37]. In this study, we found that oral administration of exogenous melatonin alleviated the symptoms of CDI in a mouse model of infection. Although determining the exact mechanism will require further investigation, we propose that the melatonin-mediated inhibition

of TcdB intoxication observed in this study might contribute to its therapeutic effect. Taken together, these results indicate that the alterations in gut metabolites caused by CAPE might also contribute to treatment outcomes for CDI patients.

Methods

Cell lines

All cell lines (HeLa, Caco-2, Vero, HEK293T and THP-1) were obtained from ATCC (Manassas, VA). HeLa, Caco-2, Vero and HEK293T cells were cultured in Dulbecco's modified Eagle's medium (DMEM) (Invitrogen, Carlsbad, CA) supplemented with 10% fetal bovine serum (FBS) (Invitrogen) and 1% (w/v) penicillin streptomycin. THP-1 cells were cultured in Roswell Park Memorial Institute (RPMI) 1640 medium (Invitrogen) supplemented with 10% FBS and 1% (w/v) penicillin streptomycin. All cell lines were cultured at 37 °C in a 5% CO_2 atmosphere.

Bacterial strains and reagents

C. difficile BAA-1870 (RT027/ST1) was kindly provided by Aiwu Wu (Guangzhou Medical University) and cultured in brain-heart infusion broth (BHI) supplemented with 5 g/L yeast extract and 0.1% (w/v) L-cysteine (BHIS). The compounds were identified from two main sources: FDA-approved drugs obtained from ApexBio Technology (Houston, TX, USA) and small molecule natural compounds obtained from Chengdu Ruifensi Biotechnology Co., Ltd.

(Chengdu, China). LysoTracker Red DND-99, kanamycin, and cefoperazone sodium were purchased from Dalian Meilun Biotechnology Co., Ltd. (Dalian, China).

Mice

Male C57BL/6 mice aged 6-8 weeks were purchased from Liaoning Changsheng Biotechnology Co., Ltd., and housed in a specific pathogen-free (SPF) facility. The mice lived in a controlled environment with a temperature of 23±2 °C and a humidity of 55±10 °C. Prior to infection, the mice were acclimated to the environment for a minimum of one week. All mouse experiments were approved by the Jilin University Institutional Animal Care Committee, Jilin University and strictly conducted according to the guidelines of this committee (SY202402301).

Protein expression and purification

The expression and purification of full-length TcdB were conducted following the method described by *Yang* et al. [64]. In brief, *Bacillus megaterium* harboring pHis1522-TcdB was inoculated into LB media supplemented with a final concentration of 10 μg/mL tetracycline. Once the $OD600_{nm}$ reached approximately 0.3, xylose (0.5% w/v) was added to induce protein expression at 37 °C for 16 h. Then, 100 mL of the bacterial cells was harvested by centrifugation, resuspended in 5 mL of lysis buffer containing 20 mM imidazole, 300 mM NaCl, 20 mM NaH_2PO_4, 500 μM EDTA, and protease inhibitor cocktail (adjusted to pH 8.0), and subjected to sonication. The cell lysate was then

560 centrifuged at 13,400 × g for 20 min to remove cell debris. The TcdB protein
561 was purified using nickel column affinity chromatography. The purity of the
562 protein was confirmed by SDS□PAGE, and the protein was subsequently
563 dialyzed against buffer containing 10% glycerol, 20 mM Tris (pH 7.5), and 150
564 mM NaCl. After the protein concentration was determined, the purified TcdB
565 protein was aliquoted and stored at -80 °C for further use.

566 For the purification of GTD, amplified DNA products were inserted into
567 pET28a (Novagen), and the *Escherichia coli* (*E. coli*) strain BL21 (DE3) was
568 used for the expression and purification of GTD. Transformed *E. coli*
569 pET28a-GTD was cultured in Luria–Bertani (LB) medium supplemented with
570 10 μg/mL kanamycin. Once the OD600 reached 0.6, the expression of proteins
571 was induced with 0.2 mM isopropyl-β-d-thiogalactoside (IPTG) overnight at
572 18 °C. The bacterial cells were then harvested by centrifugation and subjected
573 to sonication. The cell lysate was then centrifuged at 13,400 × g for 20 min to
574 remove cell debris. GTD protein was purified using nickel affinity
575 chromatography and dialyzed in buffer containing 10% glycerol, 20 mM Tris
576 (pH 7.5), and 150 mM NaCl. The GTD mutants were introduced into
577 pET28a-GTD using the Quick Change Site-Directed Mutagenesis Kit
578 (Stratagene, San Diego, CA, USA) with the primers listed in **Table S2.** The
579 subsequent purification was performed using the same procedure as
580 described for wild-type GTD.

581 **Reverse transcription-quantitative PCR**

Total RNA was extracted by TRIzol and then reverse-transcribed into complementary DNA by a NovoScript® Plus All-in-one 1st Strand cDNA Synthesis SuperMix (E047; Novoprotein, China). mRNA expression of *tcdB* was measured by quantitative PCR with NovoScript®SYBR qPCR SuperMix Plus (E096; Novoprotein, China) using the primers shown in **Table S3**. 16S rRNA was used as internal control. The relative mRNA expression levels were calculated by the delta-delta CT method.

Growth curve assays

Growth curve assay was performed to estimate the influence of CAPE on the growth of *C. difficile* BAA-1870. The overnight culture of BAA-1870 was transferred to fresh BHIS medium and incubated at 37°C in an anaerobic atmosphere. The culture was supplemented with different concentrations of CAPE ranging from 0 to 64 μg/mL and the optical density at 600 nm was monitored at 4 h intervals to assess growth of BAA-1870.

Inhibition of spore outgrowth

The impact of CAPE on the sporulation of *C. difficile* BAA-1870 was assessed using the protocol described by Joshua *et al* [65]. In brief, BAA-1870 cultures were treated with 8 or 32 μg/mL of CAPE for 48 h. The treated samples were then harvested, subjected to a double wash with PBS, and incubated in a 60°C water bath for 30 min. Subsequently, 20 μL of each spore suspension was plated onto BHIS agar supplemented with 0.1% taurine to facilitate germination. These plates were incubated anaerobically at 37°C for 5

d to allow for spore germination. Following this period, the number of resulting colonies on the plates was enumerated.

Cell rounding assay

Cell rounding assay was performed according to Kristina *et al*, with appropriate adjustments [48]. Vero or HeLa cells were seeded in 96-well sterile plates using serum-free DMEM overnight, and the compounds were preincubated with TcdB for 1 h. After incubation, the TcdB-compound complex was added to cells for 1 h at 37 °C. The cell morphology was visualized under a light microscope.

LysoTracker assay

The pH of endosomes was determined by LysoTracker Red DND-99 [49]. Caco-2 or THP-1 cells in complete DMEM were seeded in 96-well sterile plates overnight. The media was changed to serum-free DMEM for 1 h, and CAPE was preincubated with TcdB for 1 h, followed by addition to the cells and incubation for 2 h. Baf-A1 served as a control. After incubation, LysoTracker and Hoechst dyes were added and the cells were incubated for 1 h. Excess dye was removed by changing the media, and alterations in lysosomal red intensity were documented using a fluorescence microscope.

***In vitro* TcdB autoprocessing assay**

The self-cleavage ability of TcdB primarily depends on its cysteine protease activity [48]. CAPE (1-16 μg/mL) was preincubated with TcdB for 1 h, followed by the addition of $InsP_6$ and incubation at 37 °C for 6 h. Subsequently,

loading buffer was added for SDS-PAGE analysis, and the results were visualized using Coomassie Brilliant Blue staining.

Rac1 glucosylation assay

Rac1 glucosylation assay was performed following the method described by John *et al* [50]. HEK293T cells were seeded into a 6-well plate. The next day, TcdB and different concentrations of CAPE (4-32 μg/mL) were added to cells. After 2 h, the cells were harvested, lysed using lysis buffer, and subjected to centrifugation at 13,400 × g for 10 min to collect the supernatant. The collected supernatant was then mixed with loading buffer and subjected to SDS-PAGE followed by western blot analysis. The glycosylation level of Rac1 was evaluated by determining the levels of non-glycosylated Rac1 (BD Biosciences, Mississauga, ON) and total Rac1 (Abcam).

UDP-Glo™ UDP-glucose hydrolase assay

GTD activity was assessed according to the manufacturer's instructions [50]. A total volume of 16 μL, consisting of 100 nM GTD, various concentrations of CAPE and glucosylation buffer, was prepared. Four microliters of UDP-glucose at a final concentration of 25 μM was added to the mixture, which was then allowed to react at room temperature for 15 min. To stop the reaction, 10 μL of the reaction mixture was removed and placed in a white polystyrene 96-well plate containing 10 μL of UDP detection reagent. The reaction took place at room temperature for 1 h. The luminescence value was measured at a 750 ms integral, and the GTD activity was determined based on these measurements.

Circular dichroism (CD) spectroscopy

CD spectra of TcdB, TcdB-CAPE, GTD, and GTD-CAPE were obtained using a CD spectrophotometer (MOS-500; Bio-Logic, France). TcdB or GTD at a concentration of 0.2 mg/mL was incubated with 32 μg/mL CAPE. Changes in the secondary structure of TcdB or GTD were assessed at room temperature using a quartz cuvette with an optical path length of 1 mm. The scan wavelength range was set from 190 to 250 nm with a resolution of 0.2 nm and a bandwidth of 1 nm. The secondary structures of TcdB, TcdB-CAPE, GTD, and GTD-CAPE were analyzed using the BeStSel web server.

Molecular docking

CAPE was obtained as a ligand from PubChem, and its topology was generated using AmeberTools. The crystal structure of GTD was retrieved from the Protein Data Bank (PDB) and processed using AutoDockTools. Docking calculations were performed using AutodockVina, and molecular dynamics simulations were carried out using Gromacs 2020.6. The RMSD of the receptor and ligand was monitored to assess conformational changes during the binding process. The interaction energy was analyzed using the Poisson-Boltzmann surface area (MM-PBSA) method, which is a molecular mechanics approach.

Flow cytometry

Flow cytometry was used to quantify the cellular uptake of TcdB via endocytosis. To facilitate detection, full-length TcdB was labeled with Alexa

Fluor®488 NHS Ester (Yeasen Biotechnology Co., Ltd., Shanghai, China). Prior to cell treatment, Alexa Fluor 488-TcdB was preincubated with CAPE at a concentration of 32 μg/mL for 30 min. The treated solution was then added to Caco-2 cells and incubated for 1 h at 37 °C. Following three washes with phosphate-buffered saline (PBS), the Caco-2 cells were collected, and the fluorescence signal was measured using flow cytometry.

Cytotoxicity assay

Vero or THP-1 cells were plated into 96-well plates. The next day, different concentrations of CAPE were prepared by diluting them in DMEM and adding them to the cells. After incubation at 37 °C for 3 h, the viability of cells was assessed using a Cell Counting Kit-8 (CCK-8) (Beyotime Biotechnology Co., Shanghai, China) according to the manufacturer's instructions.

Biacore analysis

The affinity analysis of TcdB or GTD with CAPE was conducted using a Biacore T100 device (Biacore Inc., Uppsala, Sweden) according to the manufacturer's protocol. A CM5 chip (General Electric Company, GE) was utilized to immobilize the TcdB or GTD proteins. Various concentrations of CAPE were injected, and all steps were performed in running buffer consisting of 5% DMSO in PBS-P20 (GE). Evaluation version 3.1 software provided by Biacore and the 1:1 Langmuir combined model were employed for data analysis.

Mouse infection model

For the acute toxicity model, after pretreatment of TcdB with CAPE (2 or 4 μg/mL) for 1 h, the mice were intraperitoneally injected with a complex of TcdB-solvent or TcdB-CAPE (30 ng of TcdB per mouse). The survival of mice was observed for 72 h.

For the CDI model, mice were given cefoperazone (0.5 g/L) in their drinking water for 5 days (from day -7 to day -2), followed by switching to sterilized water for 2 days. On day 0, the mice were challenged with 1×10^8 colony-forming units (CFUs) of *C. difficile* BAA-1870 (Ribotype 027) by oral gavage. For the CAPE or melatonin treatment group, mice were treated with CAPE (30 mg/kg by oral gavage) or melatonin (200 mg/kg by oral gavage) every day after *C. difficile* challenge. The weight loss and fecal state of the mice were monitored daily. Fecal samples were collected on days 0-3 to evaluate the stool water content as a marker of diarrhea. Additionally, fecal samples on day 3 were collected to assess *C. difficile* colonization. Colonic tissues were collected on day 3 post infection, stained with hematoxylin and eosin (H&E) and scored as previously described [66].

Fecal samples were collected on day 3 post infection, frozen in liquid nitrogen and transferred to the laboratory with dry ice for 16S rRNA sequencing and untargeted metabolomics analysis (Novogene Bioinformatics Technology Co., Ltd., Tianjin, China). The melatonin level in mouse stool supernatant was determined using the Mouse MT (Melatonin) ELISA Kit (Sangon Biotechnology Co., Ltd., Shanghai, China).

Statistical analysis

Western blot densitometry and LysoTracker fluorescence intensity were measured using ImageJ software (NIH, Bethesda, MD, USA). Statistical analysis was performed using GraphPad Prism 9.0 (GraphPad Software, USA). Unpaired two-tailed Student's t tests were used for comparing two groups, and one-way analysis of variance (ANOVA) was used for analyzing data from more than three groups. The statistical significance was determined using the log-rank (Mantel–Cox) test (survival rates) and Mann–Whitney U test (tissue bacterial load) *in vivo*. All the data are expressed as the mean ± standard deviation (SD). * indicates $p < 0.05$ and ** indicates $p < 0.01$.

Acknowledgments

The authors thank Professor Aiwu Wu (Guangzhou Medical University) for the *C. difficile* BAA-1870 strain and Professor Hanping Feng (Tufts University) for the pHis1522-TcdB plasmid. This work was supported by the National Key Research & Development Program of China (2021YFD1801000), National Natural Science Foundation of China (32200141), the Natural Science Foundation of Jilin Province (20230101142JC and 20240101282JC), and The Fundamental Research Funds for the Central Universities.

Author contributions

Y.G., L.Q.H and J.Z.Q designed the study and wrote the manuscript. Y.G.,

Y.Z., G.Z.W. and H.T.L. conducted experiments. J.F.W., X.M.D., L.Q.H. and J.Z.Q. supervised the study and revised the manuscript. All authors read and approved the final manuscript. J.Z.Q. and L.Q.H. are responsible for the overall content as the guarantor.

Competing interests

The authors declare that they have no competing interests.

Data availability

All 16S rRNA gene sequencing data generated and analyzed during the current study were deposited in the Sequence Read Archive (SRA) under the BioProject accession number PRJNA1100298. Untargeted metabolomics data are available via Metabolights with the identifier MTBLS9938.

References

1. Smits WK, Lyras D, Lacy DB, Wilcox MH, Kuijper EJ. Clostridium difficile infection. *Nat Rev Dis Primers* **2**, 16020 (2016).

2. Miller BA, Chen LF, Sexton DJ, Anderson DJ. Comparison of the burdens of hospital-onset, healthcare facility-associated Clostridium difficile Infection and of healthcare-associated infection due to methicillin-resistant Staphylococcus aureus in community hospitals. *Infect Control Hosp Epidemiol* **32**, 387-390 (2011).

3. Kelly CP, LaMont JT. Clostridium difficile--more difficult than ever. *N Engl J Med* **359**, 1932-1940 (2008).

4. Dubberke E. Clostridium difficile infection: the scope of the problem. *J Hosp Med* **7 Suppl 3**, S1-4 (2012).

5. Lessa FC*, et al.* Burden of Clostridium difficile infection in the United States. *N Engl J Med* **372**, 825-834 (2015).

6. Goorhuis A*, et al.* Emergence of Clostridium difficile infection due to a new hypervirulent strain, polymerase chain reaction ribotype 078. *Clin Infect Dis* **47**, 1162-1170 (2008).

7. He M*, et al.* Emergence and global spread of epidemic healthcare-associated Clostridium difficile. *Nat Genet* **45**, 109-113 (2013).

8. Clements AC, Magalhaes RJ, Tatem AJ, Paterson DL, Riley TV. Clostridium difficile PCR ribotype 027: assessing the risks of further worldwide spread. *Lancet Infect Dis* **10**, 395-404 (2010).

9. Cornely OA*, et al.* Fidaxomicin versus vancomycin for infection with Clostridium difficile in Europe, Canada, and the USA: a double-blind, non-inferiority, randomised controlled trial. *Lancet Infect Dis* **12**, 281-289 (2012).

10. Bingley PJ, Harding GM. Clostridium difficile colitis following treatment with metronidazole and vancomycin. *Postgrad Med J* **63**, 993-994 (1987).

11. Feuerstadt P, Theriault N, Tillotson G. The burden of CDI in the United States: a multifactorial challenge. *BMC Infect Dis* **23**, 132 (2023).

12. Hopkins RJ, Wilson RB. Treatment of recurrent Clostridium difficile colitis: a narrative review. *Gastroenterol Rep (Oxf)* **6**, 21-28 (2018).

13. Spigaglia P, Mastrantonio P, Barbanti F. Antibiotic Resistances of Clostridium difficile. *Adv Exp Med Biol* **1050**, 137-159 (2018).

14. Seekatz AM, Young VB. Clostridium difficile and the microbiota. *J Clin Invest* **124**, 4182-4189 (2014).

15. Paredes-Sabja D, Shen A, Sorg JA. Clostridium difficile spore biology: sporulation, germination, and spore structural proteins. *Trends Microbiol* **22**, 406-416 (2014).

16. Lyras D*, et al.* Toxin B is essential for virulence of Clostridium difficile. *Nature* **458**, 1176-1179 (2009).

17. Kuehne SA, Cartman ST, Heap JT, Kelly ML, Cockayne A, Minton NP. The role of toxin A and toxin B in Clostridium difficile infection. *Nature* **467**, 711-713 (2010).

18. Carter GP*, et al.* Defining the Roles of TcdA and TcdB in Localized Gastrointestinal Disease, Systemic Organ Damage, and the Host Response during Clostridium difficile Infections. *mBio* **6**, e00551 (2015).

19. Drudy D, Fanning S, Kyne L. Toxin A-negative, toxin B-positive Clostridium difficile. *Int J Infect Dis* **11**, 5-10 (2007).

20. Chen P*, et al.* Structure of the full-length Clostridium difficile toxin B. *Nat Struct Mol Biol* **26**, 712-719 (2019).

21. Orrell KE, Melnyk RA. Large Clostridial Toxins: Mechanisms and Roles in Disease. *Microbiol Mol Biol Rev* **85**, e0006421 (2021).

22. Rasko DA, Sperandio V. Anti-virulence strategies to combat bacteria-mediated disease. *Nat Rev Drug Discov* **9**, 117-128 (2010).

23. Tam J, Beilhartz GL, Auger A, Gupta P, Therien AG, Melnyk RA. Small molecule inhibitors of Clostridium difficile toxin B-induced cellular damage. *Chem Biol* **22**, 175-185 (2015).

24. Balaha M, De Filippis B, Cataldi A, di Giacomo V. CAPE and Neuroprotection: A Review. *Biomolecules* **11**, (2021).

25. Garland M*, et al.* The Clinical Drug Ebselen Attenuates Inflammation

and Promotes Microbiome Recovery in Mice after Antibiotic Treatment for CDI. *Cell Rep Med* **1**, (2020).

26. Li X*, et al.* A strain of Bacteroides thetaiotaomicron attenuates colonization of Clostridioides difficile and affects intestinal microbiota and bile acids profile in a mouse model. *Biomed Pharmacother* **137**, 111290 (2021).

27. Kienesberger B*, et al.* (S)-Reutericyclin: Susceptibility Testing and In Vivo Effect on Murine Fecal Microbiome and Volatile Organic Compounds. *Int J Mol Sci* **22**, (2021).

28. Khanna S*, et al.* Gut microbiome predictors of treatment response and recurrence in primary Clostridium difficile infection. *Aliment Pharmacol Ther* **44**, 715-727 (2016).

29. Dong D*, et al.* Effects of intestinal colonization by Clostridium difficile and Staphylococcus aureus on microbiota diversity in healthy individuals in China. *BMC Infect Dis* **18**, 207 (2018).

30. Gurung B, Stricklin M, Wang S. Gut Microbiota-Gut Metabolites and Clostridioides difficile Infection: Approaching Sustainable Solutions for Therapy. *Metabolites* **14**, (2024).

31. Cronstein BN. Adenosine, an endogenous anti-inflammatory agent. *J Appl Physiol (1985)* **76**, 5-13 (1994).

32. Yong T*, et al.* Caffeic acid phenethyl ester alleviated hypouricemia in hyperuricemic mice through inhibiting XOD and up-regulating OAT3. *Phytomedicine* **103**, 154256 (2022).

33. de Araujo Junqueira AF*, et al.* Adenosine deaminase inhibition prevents Clostridium difficile toxin A-induced enteritis in mice. *Infect Immun* **79**, 653-662 (2011).

34. Neumann-Schaal M, Jahn D, Schmidt-Hohagen K. Metabolism the Difficile Way: The Key to the Success of the Pathogen Clostridioides difficile. *Front Microbiol* **10**, 219 (2019).

35. Bouillaut L, Self WT, Sonenshein AL. Proline-dependent regulation of Clostridium difficile Stickland metabolism. *J Bacteriol* **195**, 844-854 (2013).

36. Jackson S, Calos M, Myers A, Self WT. Analysis of proline reduction in

the nosocomial pathogen Clostridium difficile. *J Bacteriol* **188**, 8487-8495 (2006).

37. Sutton SS, Magagnoli J, Cummings TH, Hardin JW. Melatonin as an Antimicrobial Adjuvant and Anti-Inflammatory for the Management of Recurrent Clostridioides difficile Infection. *Antibiotics (Basel)* **11**, (2022).

38. 2019 AR Threats Report., 2019. [Available from: https://www.cdc.gov/drugresistance/biggest-threats.html].

39. Abbas A, Zackular JP. Microbe-microbe interactions during Clostridioides difficile infection. *Curr Opin Microbiol* **53**, 19-25 (2020).

40. Raplee I*, et al.* Emergence of nosocomial associated opportunistic pathogens in the gut microbiome after antibiotic treatment. *Antimicrob Resist Infect Control* **10**, 36 (2021).

41. Beilhartz GL, Tam J, Melnyk RA. Small Molecules Take A Big Step Against Clostridium difficile. *Trends Microbiol* **23**, 746-748 (2015).

42. Ranftler C*, et al.* Binding and neutralization of C. difficile toxins A and B by purified clinoptilolite-tuff. *PLoS One* **16**, e0252211 (2021).

43. Zucca M, Scutera S, Savoia D. Novel avenues for Clostridium difficile infection drug discovery. *Expert Opin Drug Discov* **8**, 459-477 (2013).

44. Kuehne SA, Collery MM, Kelly ML, Cartman ST, Cockayne A, Minton NP. Importance of toxin A, toxin B, and CDT in virulence of an epidemic Clostridium difficile strain. *J Infect Dis* **209**, 83-86 (2014).

45. Warny M*, et al.* Toxin production by an emerging strain of Clostridium difficile associated with outbreaks of severe disease in North America and Europe. *Lancet* **366**, 1079-1084 (2005).

46. Stewart D, Anwar F, Vedantam G. Anti-virulence strategies for Clostridioides difficile infection: advances and roadblocks. *Gut Microbes* **12**, 1802865 (2020).

47. Deeks ED. Bezlotoxumab: A Review in Preventing Clostridium difficile Infection Recurrence. *Drugs* **77**, 1657-1663 (2017).

48. Bender KO*, et al.* A small-molecule antivirulence agent for treating Clostridium difficile infection. *Sci Transl Med* **7**, 306ra148 (2015).

49. Chan H*, et al.* Vitamin D(3) and carbamazepine protect against Clostridioides difficile infection in mice by restoring macrophage lysosome acidification. *Autophagy* **18**, 2050-2067 (2022).

50. Tam J*, et al.* Host-targeted niclosamide inhibits C. difficile virulence and prevents disease in mice without disrupting the gut microbiota. *Nat Commun* **9**, 5233 (2018).

51. Tam J*, et al.* Intestinal bile acids directly modulate the structure and function of C. difficile TcdB toxin. *Proc Natl Acad Sci U S A* **117**, 6792-6800 (2020).

52. Tek NA, Senture SA, Ersoy N. Is Propolis a Potential Anti-Obesogenic Agent for Obesity? *Curr Nutr Rep*, (2024).

53. Schubert AM, Sinani H, Schloss PD. Antibiotic-Induced Alterations of the Murine Gut Microbiota and Subsequent Effects on Colonization Resistance against Clostridium difficile. *mBio* **6**, e00974 (2015).

54. van Nood E*, et al.* Duodenal infusion of donor feces for recurrent Clostridium difficile. *N Engl J Med* **368**, 407-415 (2013).

55. Bornet E, Westermann AJ. The ambivalent role of Bacteroides in enteric infections. *Trends Microbiol* **30**, 104-108 (2022).

56. Pike CM, Theriot CM. Mechanisms of Colonization Resistance Against Clostridioides difficile. *J Infect Dis* **223**, S194-S200 (2021).

57. Deng H*, et al.* Corrigendum: Bacteroides fragilis Prevents Clostridium difficile Infection in a Mouse Model by Restoring Gut Barrier and Microbiome Regulation. *Front Microbiol* **10**, 601 (2019).

58. Lee C*, et al.* Safety of fecal microbiota, live-jslm (REBYOTA()) in individuals with recurrent Clostridioides difficile infection: data from five prospective clinical trials. *Therap Adv Gastroenterol* **16**, 17562848231174277 (2023).

59. Gonzales-Luna AJ, Carlson TJ, Garey KW. Review Article: Safety of Live Biotherapeutic Products Used for the Prevention of Clostridioides difficile Infection Recurrence. *Clin Infect Dis* **77**, S487-S496 (2023).

60. Hasko G, Linden J, Cronstein B, Pacher P. Adenosine receptors: therapeutic aspects for inflammatory and immune diseases. Nat Rev

Drug Discov 7, 759-770 (2008).

61. Shakya AK, Naik RR, Almasri IM, Kaur A. Role and Function of Adenosine and its Receptors in Inflammation, Neuroinflammation, IBS, Autoimmune Inflammatory Disorders, Rheumatoid Arthritis and Psoriasis. Curr Pharm Des 25, 2875-2891 (2019).

62. Cavalcante IC*, et al.* Effect of novel A2A adenosine receptor agonist ATL 313 on Clostridium difficile toxin A-induced murine ileal enteritis. *Infect Immun* **74**, 2606-2612 (2006).

63. Ma N, Zhang J, Reiter RJ, Ma X. Melatonin mediates mucosal immune cells, microbial metabolism, and rhythm crosstalk: A therapeutic target to reduce intestinal inflammation. *Med Res Rev* **40**, 606-632 (2020).

64. Yang G*, et al.* Expression of recombinant Clostridium difficile toxin A and B in Bacillus megaterium. *BMC Microbiol* **8**, 192 (2008).

65. Fletcher JR*, et al.* Clostridioides difficile exploits toxin-mediated inflammation to alter the host nutritional landscape and exclude competitors from the gut microbiota. *Nat Commun* **12**, 462 (2021).

66. Reeves AE, Theriot CM, Bergin IL, Huffnagle GB, Schloss PD, Young VB. The interplay between microbiome dynamics and pathogen dynamics in a murine model of Clostridium difficile Infection. *Gut Microbes* **2**, 145-158 (2011).

Figures

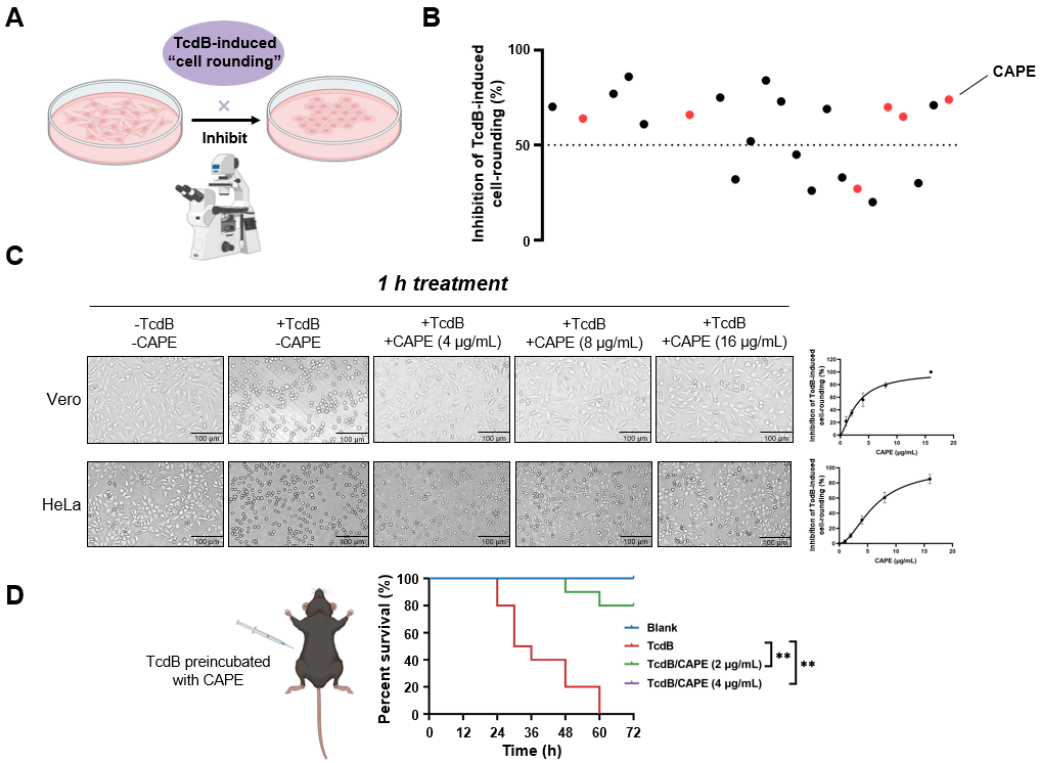

Figure 1. CAPE suppresses TcdB-mediated cell rounding.

(A) Schematic of the process used for the identification of small molecules that inhibit the cell rounding phenotype induced by TcdB. TcdB (0.2 ng/mL) was preincubated with 8 μg/mL of individual compounds prior to addition to the cell cultures. **(B)** Active compounds were identified from the chemical library consisting of 2076 chemicals. The red dots represent caffeic acid and its derivatives. **(C)** Dose-dependent CAPE inhibition of TcdB-induced rounding of Vero (upper) and HeLa (lower) cells. Scale bar, 100 μm. The dose titration curves are presented on the right. **(D)** The survival rates of mice that were intraperitoneally injected with CAPE-pretreated or native TcdB (30 ng). * p <0.05 and ** p <0.01 by log-rank (Mantel□Cox) test.

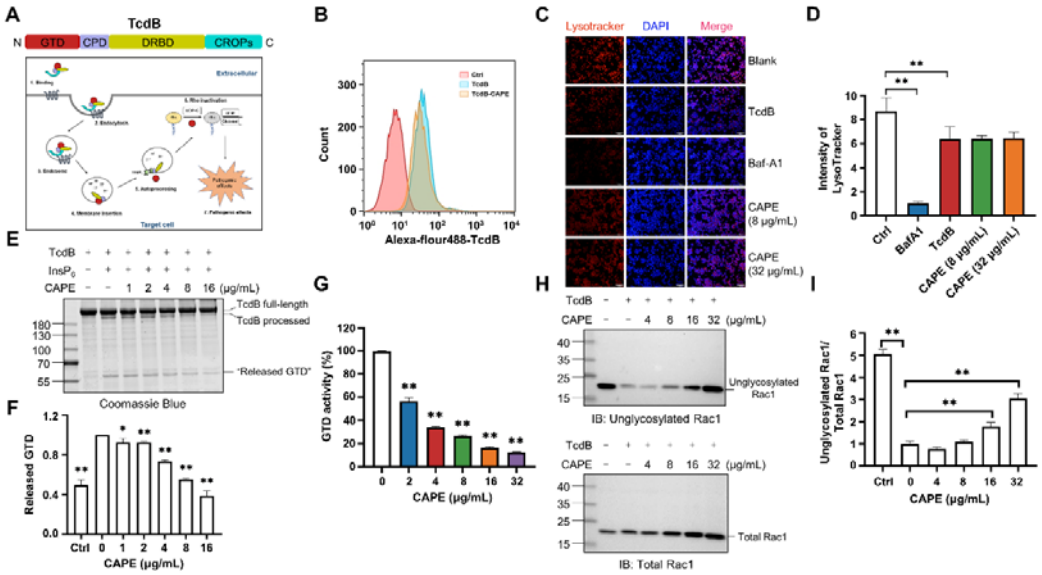

Figure 2. Mechanism by which CAPE suppresses TcdB intoxication.

(A) Schematic illustration of the multistep mechanism of TcdB intoxication of host cells. **(B)** Determination of internalized TcdB levels. Alexa Fluor 488-labeled TcdB was incubated with 32 μg/mL CAPE for 30 min before it was added to the cell culture. The cellular uptake of TcdB was measured by flow cytometry analysis. **(C)** Lysosomal activity in host cells treated with CAPE was measured via LysoTracker staining. The nuclei were stained with DAPI. Bar, 100 μm. **(D)** The intensities of LysoTracker staining were quantified using ImageJ. * p <0.05; ** p <0.01 using one-way ANOVA. **(E-F)** CAPE inhibits $InsP_6$-induced autoprocessing of full-length TcdB. Two micrograms of TcdB was preincubated with increasing concentrations of CAPE for 1 h. Self-cleavage of TcdB was initiated by the addition of 3 μg of $InsP_6$ and the cells were incubated for 6 h at 37 ^{o}C. Reactions were terminated with 5x SDS loading buffer, and the release of GTD was visualized by CBB staining of the

SDS PAGE gel **(E)**. The level of released GTD in panel E was quantified by ImageJ **(F)** * p <0.05; ** p <0.01 using one-way ANOVA. **(G)** Dose-dependent inhibition of the GTD activity of TcdB by CAPE. Recombinant GTD of TcdB was mixed with different concentrations of CAPE (0-32 μg/mL) and incubated for 15 min at 25 ^{o}C. GTD activity was measured by the UDP-Glo™ glycosyltransferase assay. **(H-I)** Intracellular Rac1 glucosylation in cells treated with TcdB. Native or CAPE-pretreated TcdB was added to the cell culture and cells were incubated for 2 h. The cells were lysed, and the glucosylation of Rac1 was analyzed by western blotting using antibodies recognizing total Rac1 and unglycosylated Rac1 **(H)**. The level of Rac1 glucosylation shown in H was quantified by ImageJ **(I)**. * p <0.05; ** p <0.01 using one-way ANOVA.

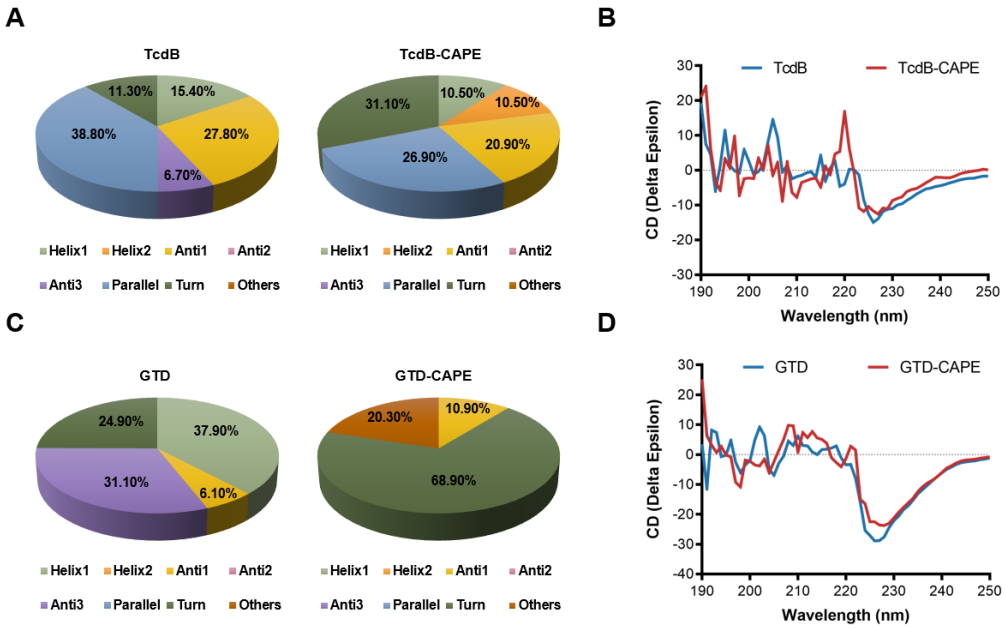

Figure 3. CAPE alters the secondary structure of TcdB and GTD.

(A) The secondary structure of TcdB in the presence or absence of 32 μg/mL CAPE was determined by CD spectroscopy. **(B)** Calculated CD spectra of CAPE-treated TcdB. **(C)** The secondary structure of GTD in the presence or absence of 32 μg/mL CAPE was determined by CD spectroscopy. **(D)** Calculated CD spectra of CAPE-treated GTD. The wavelength for CD spectroscopy was set at 190-250 nm.

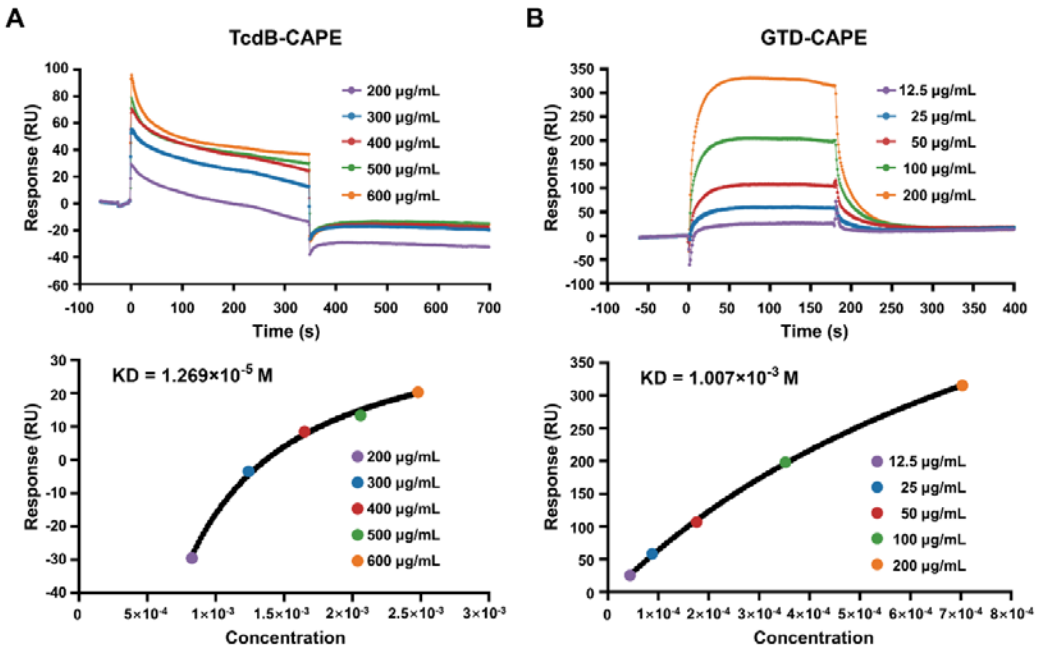

Figure 4. Direct interaction of CAPE with TcdB and GTD.

(A-B) Full-length TcdB or GTD was immobilized on a CM5 chip, followed by the injection of various concentrations of CAPE. The response unit (RU) value and affinities of CAPE interactions with TcdB **(A)** and GTD **(B)** were determined by a Biacore T100.

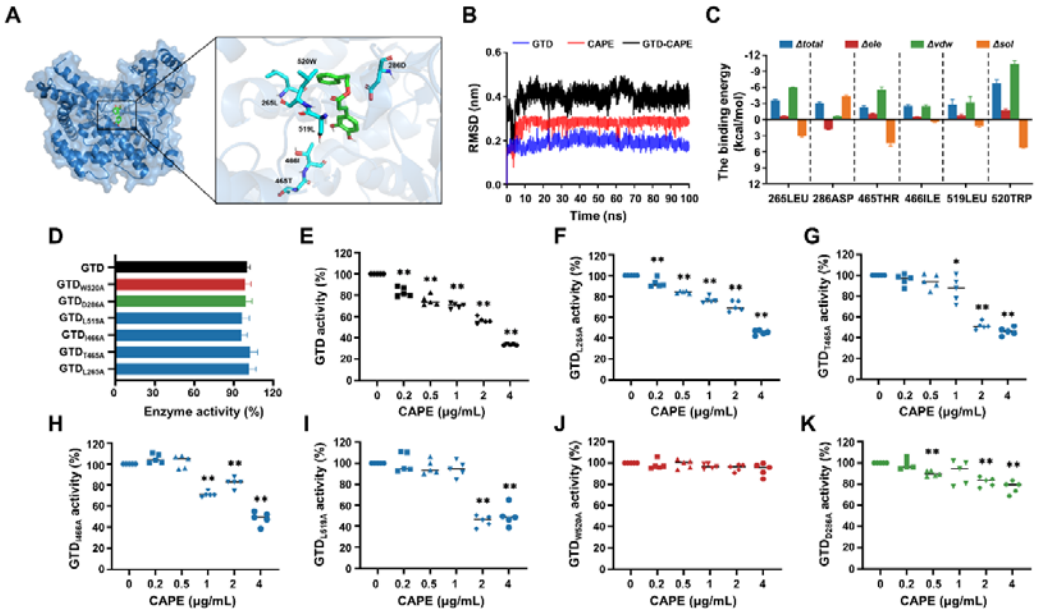

Figure 5. Asp286 and Trp520 in the GTD are critical for CAPE-mediated inhibition of GTD.

(A) Three-dimensional structure determination of GTD with the CAPE complex was performed by molecular modeling. **(B)** The RMSD values of the GTD-CAPE complex. **(C)** Decomposition of the binding energy on a per-residue basis in the binding sites of the GTD-CAPE complex. Blue denotes the total binding energy, red signifies the electrostatic interactions, green corresponds to the van der Waals forces, and orange indicates solvation or hydration effects. The horizontal axis represents the mutation of the amino acid residue at the respective position to alanine. **(D)** Glucosyltransferase activity of wild-type GTD and the GTD mutants. **(E-K)** Residual activity of wild-type GTD **(E)** and its mutants GTD_{L265A} **(F)**, GTD_{T465A} **(G)**, GTD_{I466A} **(H)**, GTD_{L519A} **(I)**, GTD_{W520A} **(J)** and GTD_{D286A} **(K)** in the presence of increasing concentrations of CAPE (0-4 μg/mL). * p <0.05; ** p <0.01 using one-way

ANOVA.

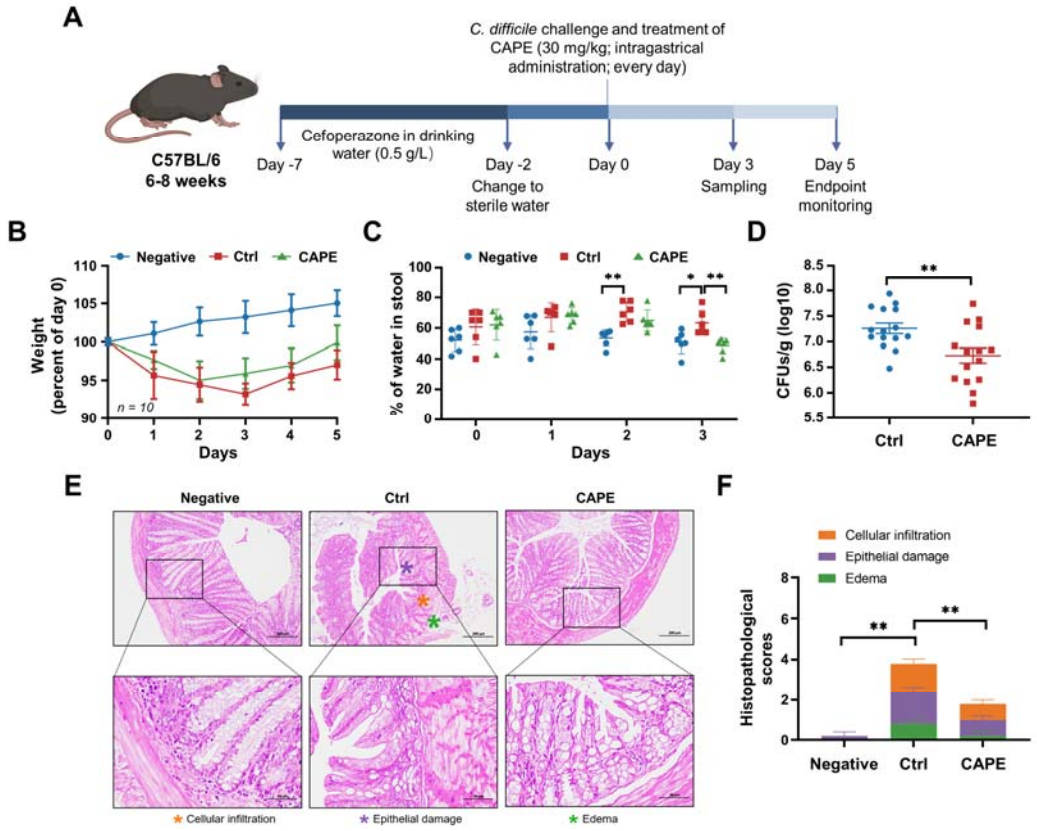

Figure 6. CAPE treatment blocks the pathology of CDI in mice.

(A) Schematic of the process used for the establishment of the CDI mouse model. **(B)** Weight changes in CDI mice after CAPE or vehicle treatment (n=10). **(C)** The fecal dry/wet weight ratio in CDI mice treated with CAPE or vehicle (n=6). * p <0.05; ** p <0.01 using one-way ANOVA. **(D)** Bacterial colonization in the feces of CDI mice treated with CAPE or vehicle (n=15). * p <0.05; ** p <0.01 using the Mann□Whitney U test. **(E)** Pathological analysis of colon sections from CDI mice treated with CAPE or vehicle. The black boxes are the regions that were magnified and are shown underneath. **(F)** Histopathological scores of vehicle-treated and CAPE-treated mice in terms of

cell infiltration (orange), epithelial damage (purple), and edema (green). * $p < 0.05$; ** $p < 0.01$ using one-way ANOVA.

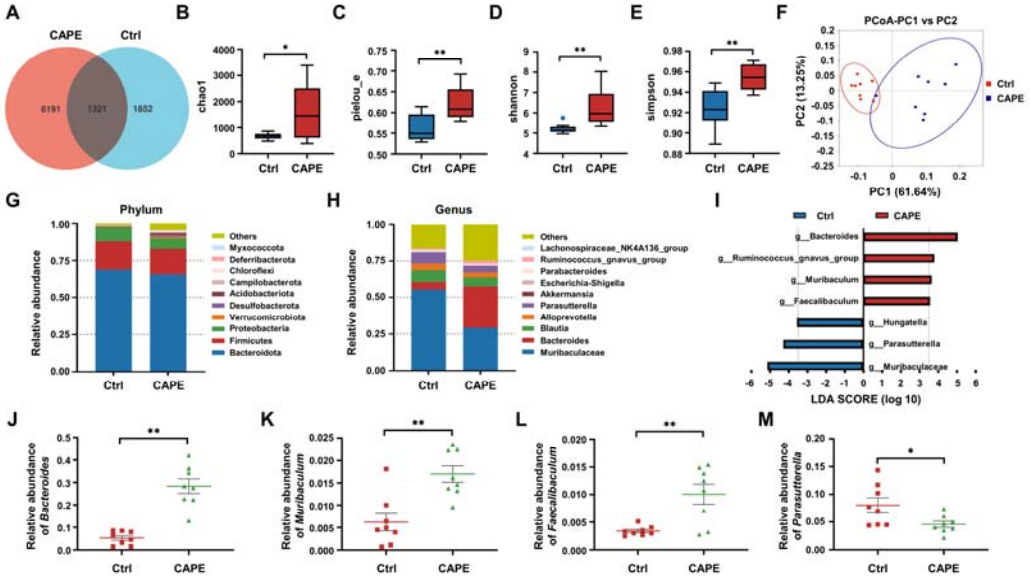

Figure 7. The influence of CAPE treatment on the diversity and composition of the gut microbiota in CDI mice.

(A) Venn diagram illustrating the numbers of differentially abundant bacteria identified using a single model and their cooperation. **(B-E)** Quantification of the α diversity of the gut microbiota according to the observed species richness **(B-C),** Shannon index **(D)**, and Simpson index **(E)**. **(F)** PCoA showing β diversity based on the weighted UniFrac distance. **(G-H)** Relative abundance of the top 10 predominant bacteria classified at the phylum **(G)** and genus **(H)** levels. **(I)** Significant changes in flora among the control and CAPE groups, as measured by LEfSe analysis (LDA score [log 10] > 3.5). **(J-M)** Relative abundances of *Bacteroides* **(J)**, *Muribaculum* **(K)**, *Faecalibaculum* **(L)**, and *Parasutterella* **(M)** in mice in the control and CAPE treatment groups. * p <0.05; ** p <0.01 using an unpaired Student's t test.

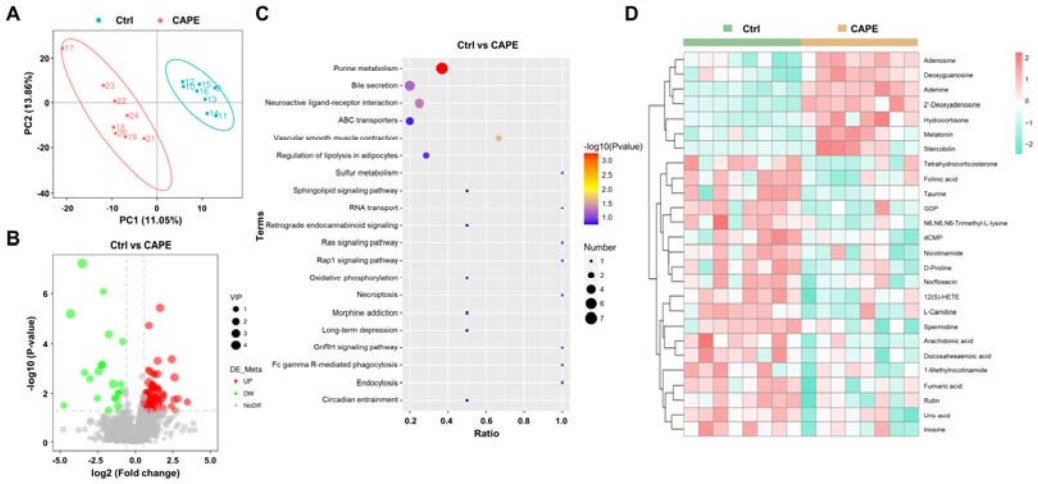

Figure 8. Alterations in gut metabolites in CAPE-treated mice with CDI. **(A)** The score plots show orthogonal partial least square discriminant analysis (PLS-DA) results. **(B)** Volcano plot representing the upregulated or downregulated gut metabolites in the CAPE treatment group compared to those in the control group. **(C)** Enrichment bubble map of the top 20 metabolic pathways in the CAPE treatment and control groups. **(D)** The 26 potential biomarkers are displayed in a heatmap, along with hierarchical clustering analysis.

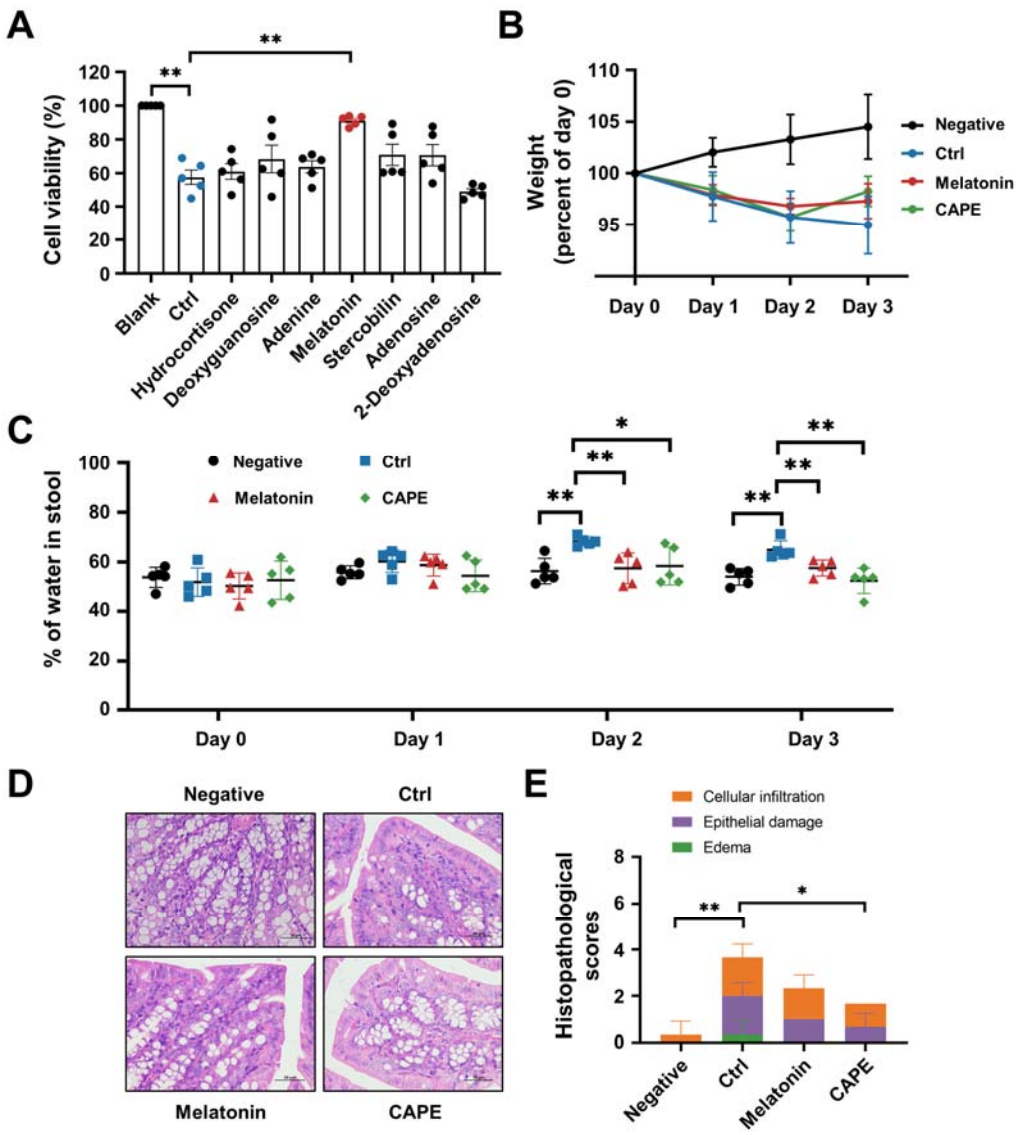

Figure 9. Oral administration of melatonin alleviates the pathology of CDI. **(A)** The impact of upregulated metabolites on the cytotoxicity of TcdB. TcdB (0.2 ng/mL) was incubated with each of the metabolites (100 μg/mL) for 1 h at 37 ^{o}C before being added to the Vero cell culture. At 3 h after TcdB treatment, cell death was evaluated with a CCK-8 kit. **(B)** Body weight changes in melatonin-treated CDI mice (n=5). **(C)** The fecal dry/wet weight ratio in CDI mice after melatonin treatment (n=5). **(D)** Histopathological analysis of colon

tissue from CDI mice treated with melatonin. **(E)** Histopathological scores of melatonin-treated CDI mice. * $p < 0.05$; ** $p < 0.01$ using one-way ANOVA.

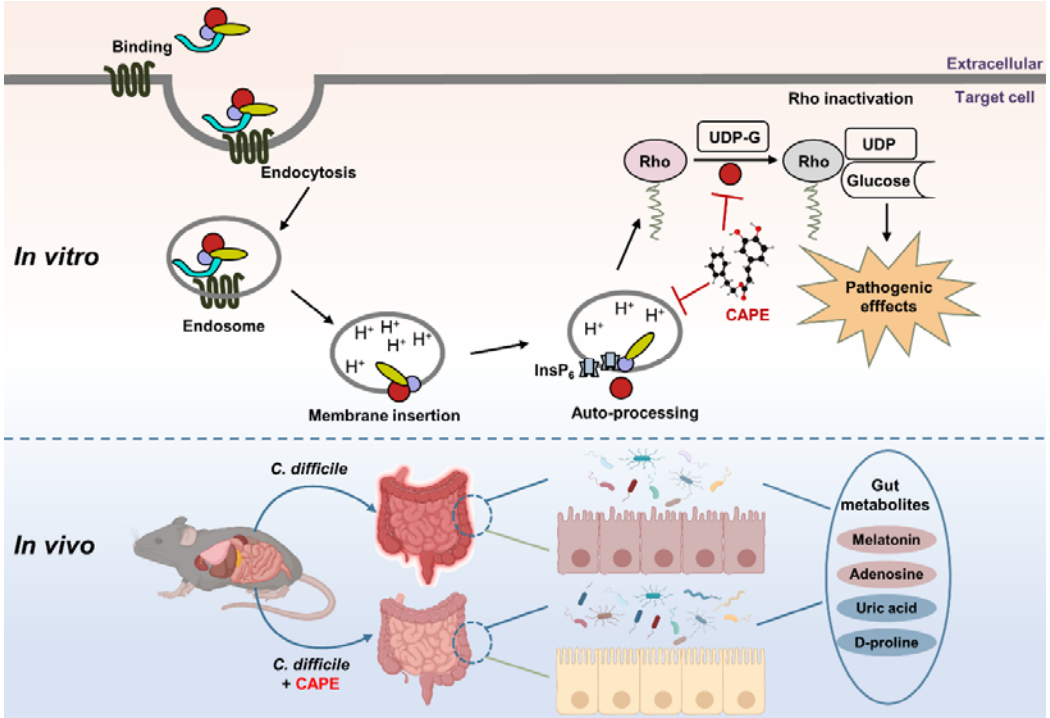

Figure 10. A model for CAPE-mediated suppression of TcdB cytotoxicity and protection of mice from CDI.

The intoxication of cells by TcdB involves multistep mechanisms. Direct interaction of CAPE with full-length TcdB blocks $InsP_6$-induced autoproteolysis, resulting in decreased production of active GTD. The binding between GTD and CAPE inhibits its glucosyltransferase activity, thus decreasing the glucosylation level of Rac1. CAPE treatment of CDI mice markedly restored the diversity and composition of the gut microbiota and induced changes in gut metabolites, which might have contributed to the therapeutic outcomes of CDI following CAPE treatment.